

Received 4 February 2025, accepted 5 March 2025, date of publication 10 March 2025, date of current version 20 March 2025.

Digital Object Identifier 10.1109/ACCESS.2025.3550012



RESEARCH ARTICLE

Glioma Brain Tumor Classification Using Convolution Neural Network and Majority Voting

PONGSAK PILAOON^{ID1}, KAZUHIKO HAMAMOTO^{ID2}, (Member, IEEE),
AND NOPPADOL MANEERAT^{ID1}

¹School of Engineering, King Mongkut's Institute of Technology Ladkrabang, Bangkok 10520, Thailand

²School of Information and Telecommunication Engineering, Tokai University, Tokyo 108-8619, Japan

Corresponding author: Noppadol Maneerat (noppadol.ma@kmitl.ac.th)

ABSTRACT Glioma brain tumors are malignant diseases for which early detection and instant treatment will increase the survival rate. Several studies have reported the efficiency of deep learning convolutional neural networks (CNN) in diagnosing brain tumors using magnetic resonance imaging (MRI). In this study, we investigated the potential of state-of-the-art classifiers to achieve the highest accuracy in the detection of brain tumors using MRI. For this purpose, we introduced a comparative study of eight state-of-the-art classifiers. The methodology comprised three different approaches: 1) an imbalanced dataset, 2) a balanced dataset using image augmentation, and 3) ensemble learning using the best of the top five models for majority hard and soft voting. The dataset comprised converted MRI data from the repository of molecular brain neoplasia data (REMBRANDT) and brain tumor segmentation 2021 (BraTS) databases. An increasing number of MRI images and datasets has prevented overfitting. Initially, a preprocessing stage morphological operation and contrast-limited adaptive histogram equalization (CLAHE) algorithms were used to remove skeletons and artifacts and optimize the image contrast for readiness classification. The stochastic gradient descent with the momentum algorithm option was used to train the network. The trained model was used to predict the testing dataset, and the results from each pretrained network were evaluated. The experimental results demonstrated that the prediction accuracy of the trained network was significantly improved using a balanced training dataset. The discriminative image region used to interpret the predicted result using the gradient-weighted class activation mapping (Grad-CAM) algorithm was proposed in the final stage for trustworthiness. The experimental results showed that the best approach was inceptionV3 with a balanced dataset. The accuracy, sensitivity, specificity, and area under the curve were 99.73%, 99.61%, 100%, and 1.00, respectively.

INDEX TERMS Glioma brain tumor, CLAHE, morphological operation, convolutional neural network, Grad-CAM, deep learning, majority voting.

I. INTRODUCTION

With a prevalence of less than 1% in the Western population, brain tumors are not very common; however, they are among the most fatal cancers. A recent study estimated the incidence rate of primary brain tumors in the United States to be

The associate editor coordinating the review of this manuscript and approving it for publication was Abdullah Iliyasu^{ID}.

approximately 0.025%; one-third of the tumors are malignant and the rest are benign or borderline malignant. Brain tumors can be classified according to their source or aggressiveness. Primary brain tumors arise in the brain, whereas metastatic brain tumors originate and spread from other cancers in the body, such as lung, colorectal, and breast cancer. The World Health Organization (WHO) classifies brain tumors into four grades based on aggressiveness and disease severity.

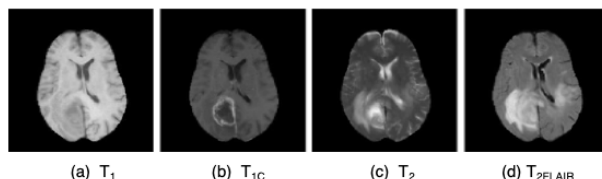


FIGURE 1. MRI image's axial slice of a high-grade glioma.

Gliomas are the most common primary brain tumors in adults, constituting 70% of all malignant primary brain tumors arising from the glial cells. They were classified into four grades. High-grade gliomas are grades III and IV malignant tumors that lead to an end of life. Grade IV gliomas are also known as glioblastoma multiforme (GBM). These are the most rapidly growing malignant primary brain tumors. These tumors infiltrated and spread along the white matter fiber tracts. Abnormal vessels and necrotic cores are observed, and surrounding edema leads to a mass effect on healthy brain tissues [1], [2].

The average survival time of patients with GBM is one year. The treatment options for gliomas include surgery, radiation therapy, chemotherapy, or a combination of these.

Magnetic resonance imaging (MRI) is a standard non-invasive technique that is widely used in clinics for brain tumor diagnosis. To produce different types of tissue contrast, varying excitation and repetition times have been applied to create a versatile tool for imaging different structures of interest. In current clinical methods, different MRI sequences are used for the diagnosis of brain tumors. These sequences or modalities include T₁-weighted MRI (T₁), T₁-weighted MRI with contrast enhancement (T_{1C}), T₂-weighted MRI (T₂), and T₂-weighted MRI with fluid-attenuated inversion recovery (T_{2FLAIR}). Fig. 1 illustrates an axial slice of the four standard sequences for a patient with glioma.

T₁-weighted MRI was used for structural analysis and easy annotation of healthy tissues. On T₁-weighted MRI with contrast enhancement, the tumor borders appeared brighter and necrotic and active tumor regions were clearly distinguished. On T₂-weighted MRI, the edematous region surrounding the tumor appeared bright. T_{2FLAIR}(FLAIR) is a special sequence that helps to separate the edema region from the cerebrospinal fluid (CSF) by increasing the time to echo (TE) and repetition time (TR); thus, the brain tumor remains bright but normal CSF is attenuated and dark. This sequence is very sensitive to pathology and makes differentiation between CSF and an abnormality much easier.

Glioma brain tumor diagnosis by medical staff is time-consuming and should be performed with medical expertise, which is a constraint in upcountry or remote areas. Therefore, this study investigated the potential of state-of-the-art classifiers to achieve the highest accuracy in brain tumor prediction using MRI. We envision the development of accurate and

effective tools to assist medical staff in classifying glioma brain tumors using artificial intelligence (AI) and computer vision techniques.

A. LITERATURE REVIEW AND ANALYSIS

Various studies on brain tumor segmentation and classification have recently been conducted using traditional machine and deep-learning algorithms, as described in Table 1. In this table, we enumerate the year of publication, methodology, datasets, performance, contributions, advantages, and disadvantages of each methodology, based on previous related studies.

Traditional machine learning and state-of-the-art deep learning methods have been applied for segmentation and classification in various studies. Traditional machine learning classification requires manual handcrafting for each stage of tumor segmentation and feature extraction before arranging the data in a tabulate for readiness to feed into each machine learning algorithm. Using this methodology, we can visually inspect the segmented tumor and select the appropriate extracted features to represent normal or tumor regions. Dataset training in a tabulate format does not require the high computer specifications. However, this method is not appropriate for applications with large datasets [3], [4], [5]. Advanced deep-learning techniques are being increasingly utilized in classification tasks. A significant advantage of deep learning is its capability to automatically extract features and segment brain tumors, a task in which traditional machine learning methods often fall short. Although convolutional neural networks (CNNs) have shown high accuracy in both segmentation and classification, they are frequently susceptible to overfitting. This problem often stems from the relatively small size of the datasets, which typically consist of images sourced from a single origin. [6], [7], [8], [9], [10], [11], [12], [13], [14]. Previous research has demonstrated impressive results in the segmentation and classification of brain tumors [15], [16], [17], [18], [19]. However, image preprocessing techniques such as morphological operations or intensity normalization may be necessary to enhance the accuracy of brain tumor detection. Furthermore, assessing the reliability of the predictions can provide a means to verify the effectiveness of the algorithm. Our proposed methodology includes preprocessing techniques that utilize morphological operations and the contrast-limited adaptive histogram equalization (CLAHE) algorithm to effectively separate the brain region from the skull and enhance image contrast. To improve accuracy, we implemented brain tumor classification using a variety of eight CNNs deep learning models along with an ensemble majority voting system based on the top five classifiers. Compared to traditional machine learning methods, our proposed approach is more suitable for large datasets of brain tumors. We aimed to prevent overfitting by combining the data from two different sources. Finally, we applied gradient-weighted class activation

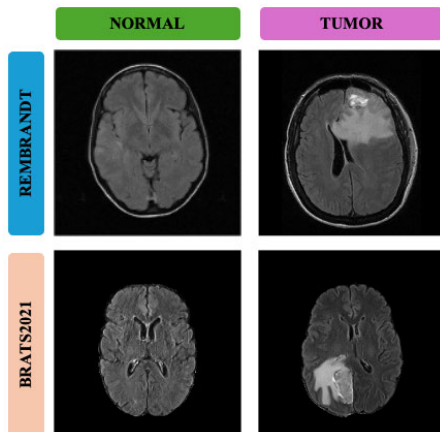


FIGURE 2. Example of MRI images from each dataset.

mapping (Grad-CAM) and local interpretable model-agnostic explanations (LIME) to visualize the regions affected by brain tumors, thereby enhancing the trustworthiness of our predictions.

II. DATASET DESCRIPTION

In this study, an MRI dataset was obtained from two sources. The first dataset used MRI images from the repository of molecular brain neoplasia data (REMBRANDT), which contained MRI images from 130 patients with clinical data analysis using digital imaging and communications in medicine (DICOM) format, and glioma grades III and IV were used for further processing [20]. The images were converted to a joint photographic expert group (JPEG) format with dimensions of $1178 \times 1177 \times 3$. In the second dataset, we utilized MRI images from brain tumor segmentation (BraTS) 2021, which contains brain glioma tumors with a pathologically confirmed diagnosis. All BraTS MRI scans are available in neuroimaging informatics technology initiative (NIfTI) file format and were exhibited with four modalities T_1 , T_{1c} , T_2 , and $T_2\text{FLAIR}$ and were acquired with different clinical protocols and various scanners from multiple data contributing institutions [21], [22], [23]. The images were converted to the JPEG format with dimensions of $1152 \times 1152 \times 3$. The MRI image from BraTS was originally intended for the segmentation of the subparts of the brain tumor, that is, the tumor core, enhancing tumor, and complete tumor. In this study, $T_2\text{FLAIR}$ modality MRI images were used to detect whole or complete tumors. The contrast between the normal brain and the tumor was distinguished, which led to easier classification. The converted JPEG images are shown in Fig. 2 and the image numbers and characteristics of each dataset are listed in Table 2. The number of original MRI images (without augmentation), training, and testing datasets are enumerated, the normal brain minority class is emphasized in bold letters, and the imbalance ratio is specified in this table.

III. METHODOLOGY

In this study, we proposed brain tumor classification using a deep learning CNN, as illustrated in the block diagram in Fig. 3. Initially, the MRI datasets were subjected to image preprocessing in morphological operations to remove the skeleton from the brain region, and artifact removal to retain the brain region only for further processing. Contrast limited adaptive histogram equalization (CLAHE) was used to balance the image contrast.

A heavily imbalanced image dataset is used in this study. To address this problem, we set up the following experimental scenarios: (i). Imbalanced dataset for training using various CNN, and (ii). Image augmentation was performed to increase the number of minority classes in the normal brain in our dataset, and the model was trained using various CNN. Finally, gradient-weighted class activation mapping (Grad-CAM) was performed to visualize the discriminative image regions for ease of understanding and interpretation. (iii). We implemented ensemble majority voting to investigate and improve the performance of brain tumor prediction. The top five prediction models were used for the majority of the hard and soft votes.

A. IMAGE PREPROCESSING

We used datasets from various sources. The difference in contrast is a normal practice, and the images also contain skeletons, noise, and artifacts that need to be removed. Therefore, image preprocessing is a prerequisite before being fed into a CNN for precise classification. We implemented image preprocessing to normalize and enhance the quality of all images as follows. A morphological operation was performed to remove skeleton, noise, and artifacts and obtain only the brain regions. Subsequently, a contrast-limited adaptive histogram equalization (CLAHE) algorithm was used for image contrast enhancement. Image preprocessing is illustrated in Fig. 4.

1) MORPHOLOGICAL OPERATION

The opening morphological operation was performed to remove the skeleton from the brain region, which is an erosion followed by dilation, using the same structuring element as the disk structuring for this study. The opening of set A by structuring element B is defined as follows:

$$A \circ B = (A \ominus B) \oplus B \quad (1)$$

Opening A by B is an erosion (\ominus) A by B followed by a dilation (\oplus) of the result obtained by B [24], [25]. First, the skeleton was removed using an opening morphological operation, and pixels in the brain region were removed. Therefore, a pixel subtraction function is used to separate the skeleton from the brain region. The open image was subtracted from the original image to obtain the skeleton and brain regions, as shown in Fig. 5b. To obtain only the skeleton, the open image (Fig. 5a) was subtracted from the skeleton with some of the brain region images obtained in the previous step. Finally, the skeleton image was subtracted from the

TABLE 1. Literature review.

Authors	Classification Methods	Dataset (image)	Accuracy	Advantages / Contribution	Disadvantages
Zaw et al. [3] Year 2019	Morphological operation to separate the brain area from the skull. The maximum entropy method was applied to enhance and obtain brain tumor images in the segmentation stage. Many morphology and intensity features were extracted from the segmented tumor area. The extracted features matrix was trained and predicted using the Naïve Bayes classifier.	REMBRANDT Tumor 90 Normal 24	Accuracy 94% Sensitivity 81.25% Specificity 100%	Developing a method to detect the brain tissues that are affected by cancer, especially for grade-4 tumor, Glioblastoma Multiforme (GBM). When compared to other methods, the significant advantage of this method is can properly detect the tumor located in different regions of the brain including the middle region which aligned with eye level that are often detected as an eye.	Segmentation tumor area and feature extraction performed by manual handcraft for each stage. Implementation with small size of the dataset which is susceptibility to overfitting.
Pilaoon et al. [4] Year 2023	This research was further developed from the previous work of Zaw et al. [3] to improve the accuracy. The methodology was composed of, preprocessing with the morphological operation to separate the brain region from the skull image and a global thresholding method was implemented for tumor segmentation. The features were extracted using a gray level co-occurrence matrix (GLCM) and a support vector machine (SVM) classifier was conducted to predict brain tumors.	REMBRANDT Tumor 111 Normal 44	Accuracy 96.875% Sensitivity 95% Specificity 100%	Proposed the automated diagnosis system to early detect GBM brain tumors. The accuracy results were significantly improved and better than the previous work. The traditional machine learning SVM was conducted to classify the represented brain tumor or normal in tabulated format. This methodology is simple and effective for manual segmentation and feature extraction. The normal computer specification is adequate for the machine learning to classify the data based on tabulated format.	Segmentation of tumor area and feature extraction were performed by manual handcraft for each stage which was time-consuming and not appropriate to implement with the large dataset. This research was implemented with the small size of the dataset which is susceptible to overfitting.
Dubey et al. [5] Year 2018	Proposed morphological and thresholding method for automatic skull stripping of the brain image. After that tumors were segmented using stationary wavelet transform (SWT), self-organizing map (SOM), and watershed algorithm. The features were extracted using a gray level co-occurrence matrix (GLCM) algorithm and were fed into feed forward neural network classifier.	Real MRI images from the Hospital, Meningioma 20, and Glioma 15 images	Accuracy 95%	Manual segmentation and feature extraction were clearly explained and applied with real MRI images from the hospital. The two tumor type meningioma and glioma were successfully classified. The proposed system can be useful for the classification of other tumor type such as lymphoma, astrocytoma, and medulloblastoma.	Segmentation of tumor area and feature extraction were performed by manual handcraft for each stage which was time-consuming and not appropriate to implement with the large dataset. This research was implemented with the small size of the dataset which is susceptible to overfitting.
Pilaoon et al. [6] Year 2023	Proposed binary classification of GBM brain tumor using convolutional neural network namely GoogLeNet and AlexNet. The actual image label was created and the stochastic gradient descent with momentum algorithm option with an initial learning rate of 0.0001 was used for the training dataset. Then the trained model was used for the prediction of the testing dataset whether a tumor or a normal brain.	REMBRANDT, Tumor 111 Normal 44	GoogLeNet, Accuracy 80.85% Sensitivity 93.94% Specificity 50% AlexNet, Accuracy 93.62% Sensitivity 96.97% Specificity 85.71%	Manual segmentation and feature extraction were automatically performed by a transfer learning network that reduced the error from human handcraft. This methodology can be implemented in practice to help the medical staff with earlier diagnosis for further treatment and increase the survivor rate of patients.	Brain tumor classification based on CNN, the raw image directly feeds into the network, and features are automatically extracted by the network. Hence, every image pixel needs to be analyzed which leads to high computer specification consumption. It seems that implemented with a small dataset which is susceptible to overfitting.

TABLE 1. (Continued.) Literature review.

Authors	Classification Methods	Dataset (image)	Accuracy	Advantages / Contribution	Disadvantages
Hossain et al. [7] Year 2019	Proposed brain tumor segmentation by fuzzy c-means clustering algorithm (FCT) and classification using different traditional machine learning, i.e., K-Nearest Neighbor, Logistic Regression, Multilayer Perceptron, Naïve Bayes, Random Forest, and Support Vector Machine. And CNN was implemented to improve the brain tumor prediction results.	BraTS dataset, Tumor 187 Normal 30	SVM, Accuracy 92.42% Sensitivity 98.3% Specificity 42.8% CNN, Accuracy 97.87%	Comparison of the accuracy of brain tumor prediction using the various traditional machine learning and CNN. In the traditional classifier part, the SVM classifier obtained the highest accuracy. Moreover, for better results, this research implemented CNN which brought good accuracy.	It seems that the dataset is small size which leads to overfitting occurrence. And the obtained accuracy results need to be further improved such as poor specificity parameter result because of the imbalanced dataset.
Dipu et al. [8] Year 2021	This paper proposed two deep learning-based approaches for brain tumor detection and classification using the cutting-edge object detection framework You Only Look Once (YOLOv5) and the deep learning library FastAi. The training directory that contained tumor and normal brain was created and utilized for training using the Google colab environment. Then the trained model was used for predicting brain tumors.	BraTS2018, 1,992 MRI images	FastAi, Accuracy 95.78% Precision 96.70% Recall 95.65% YOLOv5, Accuracy 85.95% Precision 92.67% Recall 84.33%	Comparison between two different deep learning-based approaches with good accuracy result. A large number of datasets were used for training networks with high computer specifications which led to good training and testing inference time. These two models can be applied in real-time brain tumor detection for early diagnosis of brain cancer.	Contained MRI images from BraTS 2018 single dataset only and this system will provide much better results if it were to be trained on a larger dataset for a more extended period. And the preprocessing techniques need to be implemented such as morphological operations or intensity normalization.
Arora & Sharma [9] Year 2021	Brain tumor classification using traditional machine learning. The features were extracted using the gray level co-occurrence matrix (GLCM) algorithm. The benign and malignant brain tumor was classified using SVM and Random Forest classifier. And comparative analysis with CNN transfer learning, i.e., VGG16, InceptionV3, and ResNet transfer learning.	BraTS2015, 3,764 MRI images	SVM 50.51% Random Forest 64.23% VGG16 90.54% InceptionV3 63.94% ResNet 81.92%	Brain tumor classification using different approaches with a large MRI image dataset. The work can be extended to the classification of brain tumors into different levels of malignancy. Transfer learning models are quite helpful in training medical images with very good accuracy.	It seems that overfitting problem occurrence and the obtained accuracy results needs to be further improved, and another parameter need to be evaluated such as specificity and sensitivity.
Gaikwad et al. [10] Year 2021	Preprocessing and augmentation techniques were performed before brain tumor classification using VGG-16 transfer learning. The architecture was based on CNN along with the transfer learning model VGG-16. The proposed system contained a dataset from Kaggle which was then preprocessed followed by augmentation and passed to the architecture.	Brain MRI images on Kaggle, Tumor 155 Normal 98	Accuracy 99.03%	Image augmentation was implemented for increasing and balancing the dataset before training the model which led to good accuracy obtained. The objective of this paper was to build an application of CNN by proposing a medical expert-based approach to detect brain tumor.	This study reported that time-consuming to train the model assuming that computer specification was a constraint. And another parameter needs to be evaluated such as specificity and sensitivity.
Kumar Baranwal et al. [11] Year 2020	Proposed system to classify the brain tumor images into three sub-types: Meningioma, Glioma, and Pituitary using SVM and customized CNN. Raw images are labeled and pre-processed to enhance the performance and robustness of	Nanfang and Tianjing Medical University Hospital, Meningioma : 708 Glioma : 1,426	Concluded that CNN was the best classifier, Accuracy, Meningioma: 94.12% Glioma :	The system for automatic classification of the brain tumor type based on input MRI was created. Multiclass brain tumor classification was proposed with good performance results. Three sub-types of brain tumors: Meningioma, Glioma, and	In this study, the customized CNN classifier with only one network type was proposed. Preprocessing technique to resize images from 512 x 512 to 384 x 384 pixels only. And the other

TABLE 1. (Continued.) Literature review.

Authors	Classification Methods	Dataset (image)	Accuracy	Advantages / Contribution	Disadvantages
	the model. Features were extracted using the gray level co-occurrence matrix (GLCM) algorithm before being fed into linear and polynomial SVM classifiers. Certain hyper-parameters in CNN are tuned to make the model more efficient and finally model is trained and tested.	Pituitary : 930	94.3% Pituitary : 98.85% Recall, Meningioma: 0.91 Glioma : 0.92 Pituitary : 0.99	Pituitary were classified using machine learning and CNN. Many parameters were evaluated for the performance of brain tumor classification, i.e., accuracy, precision, and recall.	preprocessing techniques need to be further implemented such as morphological operations or intensity normalization.
Aboussaleh et al. [12] Year 2021	The proposed system was divided into two phases. Firstly, The MRI image was classified into a tumor or normal by a CNN model with two neurons in the output layer, the ground truth label as tumor or normal was used in this stage. Secondly, the segmentation was applied to the images that contained the tumor using the extracted features from the last convolution layer of the proposed CNN architecture and their gradients. Finally, post-processing was applied to improve the results.	BraTS2017, High-grade glioma (HGG) 210 images Low-grade glioma (LGG) 75 images. With data augmentation the dataset was increased to 1100 labeled images, 550 for each label.	Binary classification accuracy for training (HGG+ LGG) 98%, accuracy for validation (HGG+ LGG) 91%, and segmentation with post processing (HGG+ LGG) obtained dice scores 82.35%	The strength of this approach is the intervention of a specialist to manually locate the tumor pixel by pixel because it is a complex and time-consuming task. This methodology solves these problems by using the extracted features from the CNN architecture and independently of the ground truth detected manually by specialists. The experimental results show good performance and a significant result when compared with the past related works.	This research proposed brain tumor segmentation with good performance results. However, seems that the image dataset before augmentation was a small dataset and taken from a single source only which is prone to overfitting.
Ayesha Younis et al. [13] Year 2022	Presented a binary classification of brain tumors using CNN and could be trained for faster and more convenient training using a pretrained VGG16 model. The ensemble learning was also implemented to improve the performance of brain tumor prediction.	Brain MRI images for Brain Tumor Detection Tumor 155 Normal 98	CNN 96% VGG16 98.5% Ensemble 98.14%	Various types of deep learning and ensemble learning were used for brain tumor classification. The proposed model integrated deep learning and transfer learning models to achieve a remarkable accuracy rate. The study successfully yielded better outcomes while requiring less computing time.	The preprocessing techniques need to be further implemented such as morphological operations or intensity normalization. The dataset is quite small and tends to have overfitting problems.
Hanning Hu et al. [14] Year 2021	Brain tumor detection using various CNNs to test their efficiency, including VGG16/19, AlexNet, GoogLeNet, and ResNet, and implemented a YOLO to snip the tumor's exact location. Preprocessing involves rotation, flipping, and gamma correction and is also manually labeled to train a YOLO model for detecting the tumor location. Then with the labels, two different graphic enhancement techniques were applied for cropping and color differential.	Brain Tumor Classification (MRI) dataset	ResNet50 76.904% GoogLeNet 75.38% AlexNet 74.365% VGG16 77.157% VGG19 76.396% Average 76.105%	Various CNNs were implemented for the detection of brain tumors and a web-based graphic user interface was introduced. The development of artificial intelligence in health care, and deep learning has much room to grow in the future and can further contribute to the complex medical problems of the future.	The obtained accuracy needs to be improved, and another parameter needs to be evaluated such as specificity and sensitivity. It seems that this study was implemented with a small dataset that led to overfitting occurrence. Another preprocessing technique needs to be applied such as a morphological operation to separate the skull from the brain region before feeding into the classifiers.
Pereira et al. [15] Year 2016	This paper was inspired by the work of Simonyan and Zisserman who developed	BraTS2013, BraTS2015 challenge	Dice similarity coefficient (DSC) for the	Proposed a novel CNN-based method for segmentation of brain tumors in MRI images	The proposed method was inspired by the VGG architecture. However, a

TABLE 1. (Continued.) Literature review.

Authors	Classification Methods	Dataset (image)	Accuracy	Advantages / Contribution	Disadvantages
	VGG transfer learning but this work investigate the potential of using deep architectures with small convolutional kernels for the segmentation of gliomas. The CNN with small 3x3 kernels was proposed for automatic brain tumor segmentation. And also investigated the use of intensity normalization as a preprocessing stage that aims to address data heterogeneity caused by multi-site and scanner acquisitions of MRI images.	dataset	complete, core and enhancing regions respectively. BraTS2013 0.88, 0.83, and 0.77 BraTS2015 0.78, 0.65, and 0.75	with a small 3x3 kernels CNN. The intensity normalization preprocessing technique influenced to achievement of good segmentation. In the BraTS challenge 2013, the proposed method was ranked in the first position in the DSC metric in the complete, core, and enhancing regions segmentation. And able to reduce the computation time approximately ten-fold.	significant issue with this type of network is the vanishing gradient problem. Many architectures have been developed to address this issue, resulting in improved performance, such as ResNet, Inception, and DenseNet.
Hareem Kibriya et al. [16] Year 2021	Presented multiclass brain tumor classification using deep learning and machine learning techniques. First, the MRI images were classified via CNN models, i.e., ResNet18 and GoogLeNet. The extracted features from the CNN models are also classified using SVM. MRI Images were preprocessed based on the min-max normalization technique and augmented against imbalanced dataset issues.	Public available Figshare dataset, Meningioma : 708 Glioma : 1,426 Pituitary : 930	GoogLeNet + SVM Accuracy 97.6% Precision 97.3% Recall 97.3% ResNet18 + SVM Accuracy 98% Precision 98.3% Recall 98%	Image preprocessing and augmentation were performed to normalize and balance the dataset before being fed into CNN transfer learning. SVM-classified deep feature vectors from the dedicated CNNs were applied and it was observed that the proposed system's accuracy increased when SVM was used instead of the softmax layer of CNN.	Another preprocessing technique needs to be applied such as a morphological operation to separate the skull from the brain region before feeding into the classifiers. The visualization and trustworthiness of classification need to be further investigated.
Ahmed Wasif Reza et al. [17] Year 2023	Propose the multiclass brain tumor classification using modified VGG16 architecture with 3 different classes. Preprocessing stage by resizing, orienting, and coloring before training. The proposed model is composed of 21 layers, where the first 20 layers use the rectified linear unit (ReLU) function, and the last one is the SoftMax function. And used dropout layers to reduce overfitting, the model applied 20% dropout which gave the most accurate values.	Public available Kaggle and Figshare	Glioma : 98.98% Meningioma: 99.13% Meningioma : 99.13% Pituitary : 99.95% Pituitary : 2,658 No tumor : 99.81% Overall : 99.5%	The proposed model was implemented with a large number of real datasets without augmentation and obtained remarkable results when compared to other related work. Using a modified VGG-16 architecture on 10,153 MRI images with 3 different classes, the network performs significantly well.	The significant limitation of this model is that it is comparatively slow as it contains high numbers of parameters. Additionally, this model cannot detect the exact location of the tumor.
S. Asif et al. [18] Year 2022	The MRI images were preprocessed (cropping, resizing, splitting, and normalization) and then data augmentation was used to increase the size of the dataset. The various deep transfer learning (Xception, NasNet Large, DenseNet121, and InceptionResNetV2) was implemented for detecting brain tumors with different optimizers, i.e., adaptive moment estimation (ADAM), root mean squared propagation (RMSprop), and stochastic gradient descent (SGD).	Brain Tumor Detection (large) Tumor 1500 Normal 1500 Brain MRI Images Dataset (small) Tumor 155 Normal 98	MRI large dataset with Xception and ADAM optimizer was better than the other, Accuracy 99.67% Sensitivity 99.68% Specificity 99.66%	Demonstrated the effectiveness of brain tumor classification using various CNN and different optimizers and comparison results between small and large datasets for robustness testing. The MRI images were improved during the preprocessing phase and various techniques such as data augmentation, three different optimizers (ADAM, SGD, and RMSprop), and the L2 regularizer were used to improve performance.	Another preprocessing technique needs to be applied such as a morphological operation to separate the skull from the brain region before feeding into the classifiers. The transparency and trustworthiness of prediction shall be further implemented such as Grad-CAM for discriminative image regions.

TABLE 1. (Continued.) Literature review.

Authors	Classification Methods	Dataset (image)	Accuracy	Advantages / Contribution	Disadvantages
S. Mohsen et al. [19] Year 2023	Presented glioma and pituitary brain tumors classified using ResNext101_32×8d and VGG19. A single-image super-resolution (SISR) technique was applied to the MRI images to improve their resolution before classification. The SISR consists of two phases: generator and discriminator. The ResNext101_32 ×8d model consists of 344 layers including 104 batch normalization layers, 104 conv-layers, 100 ReLU layers, 33 bottleneck layers, a single max-pooling layer, a single adaptive average layer, and one linear layer.	Brain Tumor dataset on Kaggle, Glioma : 900 Pituitary : 900	VGG19 Accuracy 99.98% Precision 99.90% Recall 99.89% ResNext101 Accuracy, Precision, and Recall was all 100%	The SISR technique based on a generative adversarial network (GAN) algorithm was implemented to improve the resolution and led to obtaining the impressive accuracy result. The Models could assist specialist doctors by providing a fast identification of patients with brain tumors, which makes these models useful tools for rapid screening and providing support for medical diagnoses.	The preprocessing MRI images shall be implemented to separate the brain region from the skeleton. The detected tumor with discriminative image region methodology shall be considered.
Our proposed method	Preprocessing techniques with various 8 CNNs and ensemble majority voting. Finally, InceptionV3 with a balanced dataset is the best classifier.	REMBRANDT and BraTS2021 dataset, Tumor 1285 Normal 571	Accuracy 99.73% Sensitivity 99.61% Specificity 100% Area under the ROC curve (AUC) 1.00	The performance was significantly improved and implemented Grad-CAM algorithm for trustworthiness.	In future work, the transformer-based models for the 3D medical images approach will be investigated to improve the performance.

TABLE 2. Converted MRI image to JPEG format from each dataset.

Dataset	MRI image (original)		Training (80%)		Testing (20%)		Remark
	Normal	Glioma	Normal	Glioma	Normal	Glioma	
REMBRANDT, Dimension 1178 x 1177 x 3	468	190	374	152	94	38	MRI images from two institutes, Thomas Jefferson University and Henry Ford Hospital. The tumor grades were justified by information from 3 radiologists and many factors were considered such as tumor location, enhancement quality, lesion size, and etc. In this study, we used malignant glioma brain tumor grades III and IV for proceeding.
BraTS2021, Dimension 1152 x 1152 x 3	103	1095	82	876	21	219	MRI image from this dataset was originally intended for segmentation tasks, but in this study, we intend to use FLAIR image type for classification of the whole tumor or complete tumor that contains tumor core and enhancing tumor inside.
Total	571	1285	456 (1:2.25)	1028	115	257	Normal brain is a minority class with ratio 1:2.25

original image and the brain region was obtained only for further processing. The morphological operation procedure is illustrated in Fig. 5.

MRI images from the REMBRANDT database were subjected to morphological preprocessing to obtain only the brain regions, as per the aforementioned steps. MRI images from the BraTS2021 database were similarly performed to remove some artifacts, and brain regions were obtained only

because MRI images from BraTS2021 were provided without a skeleton.

2) CONTRAST LIMITED ADAPTIVE HISTOGRAM EQUALIZATION (CLAHE)

The CLAHE algorithm was developed and improved from adaptive histogram equalization (AHE) for contrast enhancement of medical images [26], [27]. In this study, the dataset

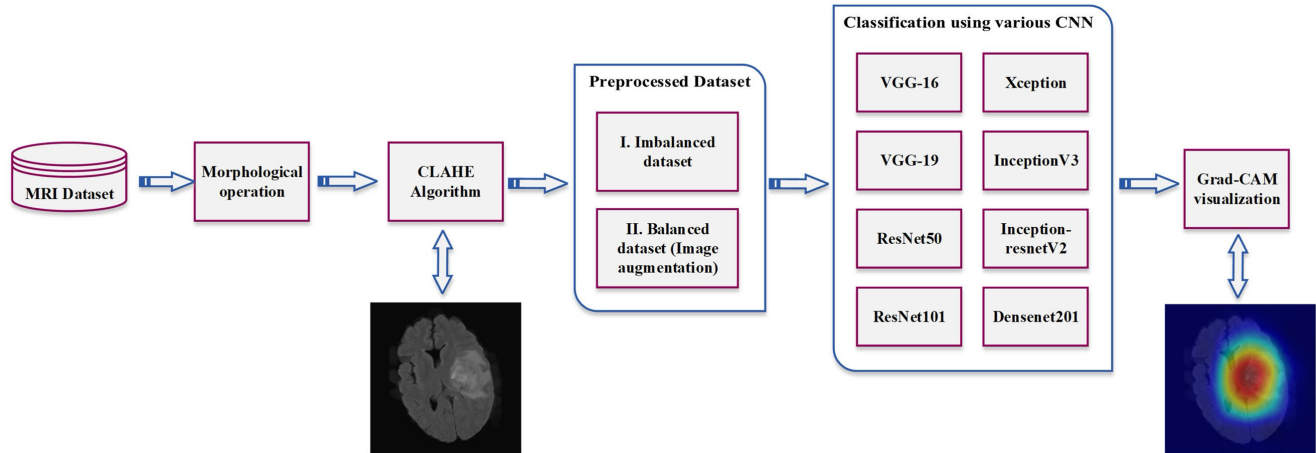


FIGURE 3. Overall block diagram of proposed methodology.

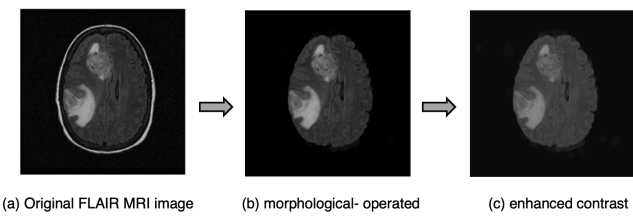


FIGURE 4. Image preprocessing for removal the artifacts and contrast enhancement.

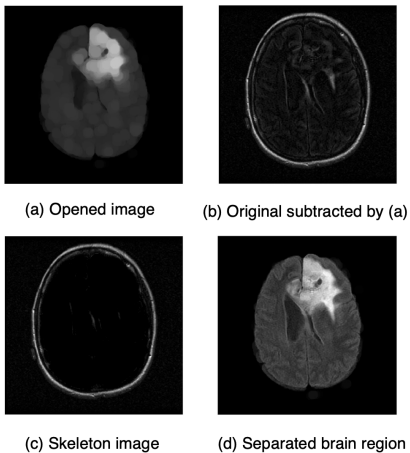


FIGURE 5. Morphological operation preprocessing.

was obtained from different sources, which led to variations in the contrast and intensity. Therefore, contrast enhancement using the CLAHE algorithm improved and normalized the image before the classification process. The CLAHE algorithm comprises of three major parts: tile generation, histogram equalization, and bilinear interpolation. Histogram equalization comprises five steps: histogram computation, excess calculation, excess distribution, excess redistribution, and scaling and mapping using a cumulative distribution

function (CDF), as shown in Equation 2.

$$\begin{aligned} S_k = T(r_k) &= (L-1) \sum_{j=0}^k p_r(r_j) \\ &= \frac{(L-1)}{MN} \sum_{j=0}^k n_j \quad k = 0, 1, 2, \dots, L-1 \end{aligned} \quad (2)$$

where $T(r_k)$ is the histogram equalization transformation, MN is the total number of pixels in the image, n_j is the number of pixels with intensity r_j , and L is the number of possible intensity levels in the image.

The original and contrasted enhancement images of the brain tumor medical image, with a histogram for each image, are illustrated in Fig. 6.

3) IMAGE AUGMENTATION FOR BALANCING THE TRAINING DATASET

In this study, the image dataset was heavily imbalanced, and previous studies demonstrated that the distribution of the training data has a significant impact on the performance of the CNN. Hence, we implemented image augmentation to increase the number of minority class images in the training dataset [28], [29], [30]. Simple augmentation rotation, reflection, synthetic noise, and synthetic blur were applied to the minority class, which was a normal brain image for our dataset. Medical MRI images of the normal brain from REMBRANDT were augmented using rotation, whereas normal brain MRI images from BraTS2021, which was the minority, were augmented using the rotation and reflection method to increase the number of training datasets.

The selected images from both datasets were further subjected to synthetic noise and blur augmentation to equalize the normal and brain tumors of the training dataset, the details of which are listed in Table 3. In this study, image augmentation was performed to increase and balance the training dataset, which is adequate for the procedure.

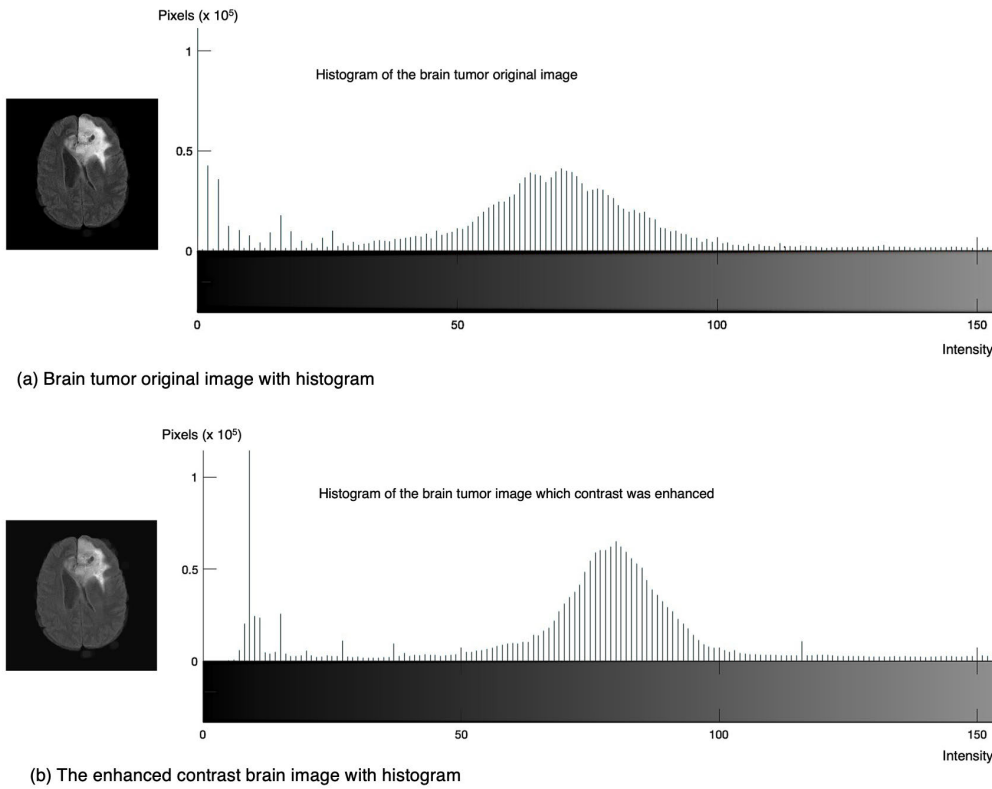


FIGURE 6. CLAHE algorithm to enhance contrast of brain MRI image.

B. VARIOUS DEEP LEARNING PRETRAINED CNNS FOR CLASSIFICATION BRAIN TUMOR

In this study, various pretrained CNNs were implemented for classification tasks. The advantage of transfer learning is that networks can learn rich feature representations from a wide range of images. The network takes images as input and ground truth labels for training, the feature is automatically extracted, and the output label is predicted. Fine-tuning a network using transfer learning is faster and easier than training from scratch. The transfer learning network comprises a pretrained network layer, training dataset, and algorithm options.

The convolution operation is denoted by an asterisk (*).

$$s(t) = (x * w)(t) \quad (3)$$

where x is often referred to as the input and the second argument is the kernel. The output is the same-time, which is referred to as a feature map.

If we use a two-dimensional image I as the input, we also want to use two-dimensional kernel K .

$$\begin{aligned} S(i, j) &= (I * K)(i, j) \\ &= \sum_m \sum_n I(m, n) K(i - m, j - n) \end{aligned} \quad (4)$$

In this study, stochastic gradient descent with momentum (SGDM) with an initial learning rate of 0.0001 was set up as the algorithm option [31]. The stochastic gradient descent

with momentum (SGDM) is described in equations (5), (6), and (7), where ϵ is the learning rate, $x^{(i)}$ is the input image, $y^{(i)}$ is the label, and θ is the weight. Firstly, compute gradient estimate.

$$g = \frac{1}{m} \nabla_{\theta} \sum_{i=1}^m L(f(x^{(i)}; \theta), y^{(i)}) \quad (5)$$

And then compute the updated velocity.

$$v \leftarrow \alpha v - \epsilon \nabla_{\theta} \left(\frac{1}{m} \sum_{i=1}^m L(f(x^{(i)}; \theta), y^{(i)}) \right) \quad (6)$$

where α is the momentum parameter. And the updated weight is computed.

$$\theta \leftarrow \theta + v \quad (7)$$

The velocity v accumulates the gradient elements g , ($v = \alpha v - \epsilon g$).

We implemented state-of-the-art pretrained network layers, viz., VGG16, VGG19 [32], ResNet50, ResNet101 [33], Xception [34], InceptionV3 [35], InceptionResNetV2 [36], and Densenet201 [37]. The properties of each network are listed in Table 4. All input images were converted to red, green, and blue (RGB) type before being used for training by the algorithms.

In this study, we investigated brain tumor prediction using state-of-the-art transfer learning methods. Recently, several

TABLE 3. Image augmentation for normal brain minority class.

Augmentation	Characteristic	Augmented MRI image	Dataset applicable	
			REMBRANDT	BraTS2021
Normal brain for training (original)	-		374	82
Rotation 90 degree			374	82
Reflection around x axis			-	82
Synthetic noise			10	7
Synthetic blur			10	7

TABLE 4. The CNN transfer learning properties used in this study.

CNNs	Layers	Parameters (x 10 ⁶)	Input Size
VGG16	16	138	224 x 224
VGG19	19	144	224 x 224
ResNet50	50	25.6	224 x 224
ResNet101	101	44.6	224 x 224
Xception	71	22.9	299 x 299
InceptionV3	48	23.9	299 x 299
InceptionResNetV2	164	55.9	299 x 299
Densenet201	201	8.1	224 x 224

CNNs transfer learning methods have been introduced and demonstrated superior results in medical image classification. We intended to use CNNs, which are the latest architectures, or obtained very good accuracy in a previous related work. The details of each CNN implemented in this study are as follows:

1) VISUAL GEOMETRY GROUP (VGG16, VGG19)

The Visual Geometry Group is a section of the Science and Engineering Department of Oxford University. VGG has

been applied in facial recognition and image classification, including VGG16 and VGG19. The researcher intended to understand how the depth of the CNN network layer affects classification accuracy. To avoid a large number of parameters, small CNN kernels (3×3) are applied to each layer. The CNN comprises an input layer, output layer, and many hidden layers. VGG16 is a CNN that has been accepted for its excellent performance in computer vision applications. This characteristic is determined by the depth of the layer, which comprises 16 layers, i.e., convolutional 13 layers, max pooling 5 layers, and fully connected 3 layers. A significant improvement in VGG is that the convolution kernel is reduced to 3×3 and the convolution layer is increased. VGG19 is improved from the VGG model and comprises 19 layers and a structure similar to VGG16, but the difference is that the depth of the layer is increased to improve the classification accuracy [32].

2) RESIDUAL NETWORK (RESNET50, RESNET101)

The researcher understood that if we increase the depth of the network layer, the accuracy would improve accordingly. However, when the layer of the network is increased to a limit point, its performance is reduced, which is a bottleneck for the VGG model because we cannot create the network layer as per the requirement because it will lose some

performance. A significant problem that ResNet can resolve is the vanishing gradient that occurs when the network layer has a depth greater than the limit by creating a shortcut in the network, which leads to a residual network structure [33].

3) XCEPTION

The Xception convolutional neural network was developed by Google researchers and modified from InceptionV3 to improve classification performance. It was assumed that the mapping of cross-channel correlations and spatial correlations in the feature map of the CNN could be separated (entirely decoupled) because of this assumption as a concentrated version of inception. Thus, Xception is abbreviated from extreme inception based on depthwise separable convolution layers (a depthwise convolution followed by a pointwise convolution). In conclusion, the Xception architecture is a linear connection of depth-wise separable convolution layers combined with a residual network layer to troubleshoot the vanishing problem [34].

4) INCEPTIONV3

InceptionV3 was developed using InceptionV1 (GoogLeNet). The concept is to use multiple filters of different sizes within the same layer, instead of simply increasing the layer depth. The layer is connected in parallel, which leads to an increase in network width. The performance of InceptionV3 was better than that of the previous version, and the architecture was modified as follows:

To reduce the convolution size, a spatial filter size of 5×5 for InceptionV1 was replaced by two convolutions with a filter size of 3×3 to reduce the computation time and cost and improve the classification performance.

Spatial factorization, in terms of asymmetric convolution, was implemented to reduce computational cost. Hence, the symmetric convolution size $n \times n$ was replaced by a convolution of $1 \times n$, followed by $n \times 1$. Although the network layer size of InceptionV3 was increased to 42 layers, the computational cost was higher than GoogLeNet by only 2.5 times and the performance was better than that of VGG [35].

5) INCEPTIONRESNETV2

InceptionResNetV2 was further developed and improved using the inception architecture, which is a combination of a residual network and a precise classification network, as mentioned in the previous section. InceptionResNetV2 was developed from the latest version of InceptionV4 and combined with a residual network to exploit the advantages of each model to improve performance. The architecture comprises layers such as the stem, inception-ResNet-A, -B, and -C, and reductions A and B [36].

6) DENSELY CONNECTED CONVOLUTIONAL NETWORKS (DENSENET201)

DenseNet is a feedforward CNN architecture that connects each layer to every other layer. For each layer, the feature

maps of all the preceding layers were used as inputs, and their feature maps were used as inputs for all subsequent layers. DenseNet offers several advantages. It alleviates the vanishing gradient problem, strengthens the feature propagation, encourages feature reuse, and substantially reduces the number of parameters. DenseNet achieves significant improvements over the state-of-the-art on most of them, while requiring fewer parameters and less computation to achieve a high performance [37].

C. GRADIENT-WEIGHTED CLASS ACTIVATION MAPPING (GRAD-CAM) FOR VISUALIZATION

In this study, we implemented a gradient-weighted class activation map (Grad-CAM) to visualize the predicted results of the classifier in the final stage and interpret more transparency by producing visual explanations. The visualization algorithm can discriminate between classes more accurately, reveal the trustworthiness of a classifier, and identify bias in datasets [38], [39]. Grad-CAM uses the gradient information flowing into the last convolutional layer of the CNN so that it can be used to visualize any activation in a deep network. To obtain a class-discriminative localization map, Grad-CAM. Initially, the class score for the output class c in the class activation maps (CAM) model y^c is given by.

$$y^c = \sum_k \alpha_k^c \frac{1}{Z} \sum_i \sum_j A_{ij}^k \quad (8)$$

where α_k^c is the weight corresponding to class c for the k feature map, A_{ij}^k is the pixel at location i, j in the k feature map, and Z is the total number of pixels in the feature map. Grad-CAM is a generalization that overcomes the limitation of class activation maps (CAM), which is the overhead of learning weights for linear mapping. The Grad-CAM weight was calculated as follows:

$$\alpha_k^c = \frac{1}{Z} \sum_i \sum_j \frac{\partial y^c}{\partial A_{ij}^k} \quad (9)$$

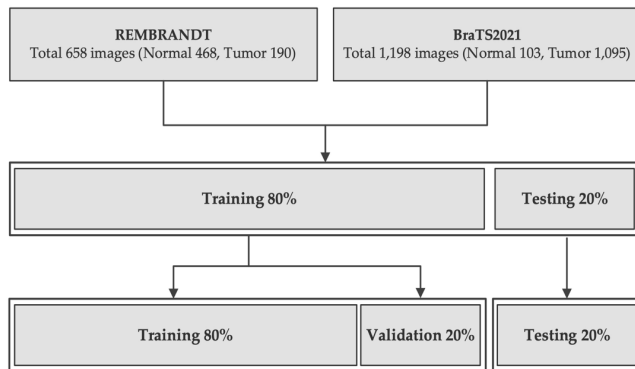
The rectified linear unit (ReLU) function was applied to the weighted combination of feature maps to retain only positive correlations in the final activation map. Finally, the class discriminative localization map Grad-CAM was obtained.

$$L_{Grad-CAM}^c = ReLU \left(\sum_k \alpha_k^c A_{ij}^k \right) \quad (10)$$

IV. EXPERIMENTAL SETUP

A. EXPERIMENTAL AND TRAINING SETUP

The brain tumor dataset used in this study was obtained from two databases. The REMBRANDT database contains MRI images from 130 patients with clinical data analysis in DICOM format. Brain tumors in different locations and normal brains in the axial FLAIR modality were obtained for classification [20]. The 658 MRI images from REMBRANDT comprised grade III and IV brain tumor 190 images and normal brain 468 images were combined

**FIGURE 7.** Dataset combination for brain tumor classification.

into a dataset. In the second database, MRI images were obtained from BraTS2021, which contains multi-institutional MRI scans in NifTI format [21], [22], [23]. The MRI image T₂FLAIR modality in the BraTS2021 database was converted to JPEG format comprising 1,198 images, including 1,095 brain tumors, and 103 normal brain images were combined in the dataset. The total combination of MRI images from the two databases contained 1,856 images comprising of brain tumor 1,285 images and normal brain 571 images were utilized for classification using various CNNs. The dataset was divided into training and testing datasets with ratios of 80% and 20%, respectively, and the brain tumor and normal images were equally distributed into the training and testing datasets. Therefore, we obtained 1,484 images for the training dataset, comprising 1,028 tumor images and 456 normal brain images, whereas the testing dataset contained 372 images, comprising 257 tumor images and 115 normal brain images. The training dataset was divided into training and validation datasets with ratios of 80% and 20%, respectively, before being used for training with the various CNNs. The dataset combination and management are shown in Fig. 7. The training dataset was heavily imbalanced. To address this issue, image augmentation is implemented to increase the number of minority classes. Therefore, the normal brain images were augmented using 90-degree rotation, reflection around the x-axis, synthetic noise, and synthetic blur for the training dataset only. The number of images obtained using each approach is listed in Table 5. In this study, we performed preprocessing and classification using MATLAB R2023a with image processing and a deep learning toolbox.

1) APPROACH 1 TRAINING ALGORITHM USING IMBALANCED DATASET

A dataset comprising 1,484 images was utilized for training using various deep-learning CNNs. A label was provided for each image, and the ground truth table specified the actual class of the brain image, that is, tumor or normal. The consistency of the brain image, image labeling, and ground-truth table was considered because it led to precise feature extraction and classification. The training dataset was divided into training and validation datasets with ratios of 80% and

TABLE 5. Dataset combination for each approach.

Approach	Dataset	Normal	Glioma	Total
Approach 1 Imbalanced dataset	Training	456	1,028	1,484
	Testing	115	257	372
Approach 2 Balanced dataset	Training	1,028	1,028	2,056
	Testing	115	257	372

20%, respectively. Transfer learning using CNNs involves training data, network layers, and algorithms. A pretrained network layer with the modified last 3 layers was used in our study. A block diagram for training the network using transfer learning is shown in Fig. 8.

The algorithm option was aligned as follows: stochastic gradient descent with momentum (SGDM), initial learning rate 0.0001, and 20 epochs for training. The network was trained using these parameters. Finally, we obtained a trained network that was utilized to predict the 372 images of the testing dataset. Training progress and confusion charts were plotted for monitoring purposes.

2) APPROACH 2 TRAINING ALGORITHM USING BALANCED DATASET

Image augmentation to increase the number of images of minority classes, balance the training datasets, and significantly improve the accuracy is a simple and effective methodology. Therefore, we performed augmentation of the normal image in the training dataset because it is heavily imbalanced as explanation in Table 3. Finally, we obtained normal brain 1,028 images and glioma brain tumor 1,028 images for utilization in the training network. The network layer and algorithm option parameters were maintained as in approach 1. Training progress was plotted for monitoring purposes. The testing dataset was maintained similar with a previous approach, that is 372 images comprising 115 normal brain images and brain tumor 257 images. The trained network was utilized for the prediction testing dataset, and the accuracy of the prediction between the predicted result and ground truth table was evaluated. A block diagram for training the balanced dataset is illustrated in Fig. 9.

3) ENSEMBLE LEARNING USING MAJORITY VOTING

Recently, several related studies have introduced ensemble learning to further improve the accuracy of medical image classification [29], [40], [41]. In this study, ensemble hard and soft majority voting were conducted to investigate the performance of brain tumor classification. The top five performance models from the previous section included the majority of the hard and soft votes. The details of the majority voting approach are as follows.

Majority hard voting: Summing the per-class predicted labels from every classifier for the input image and obtaining

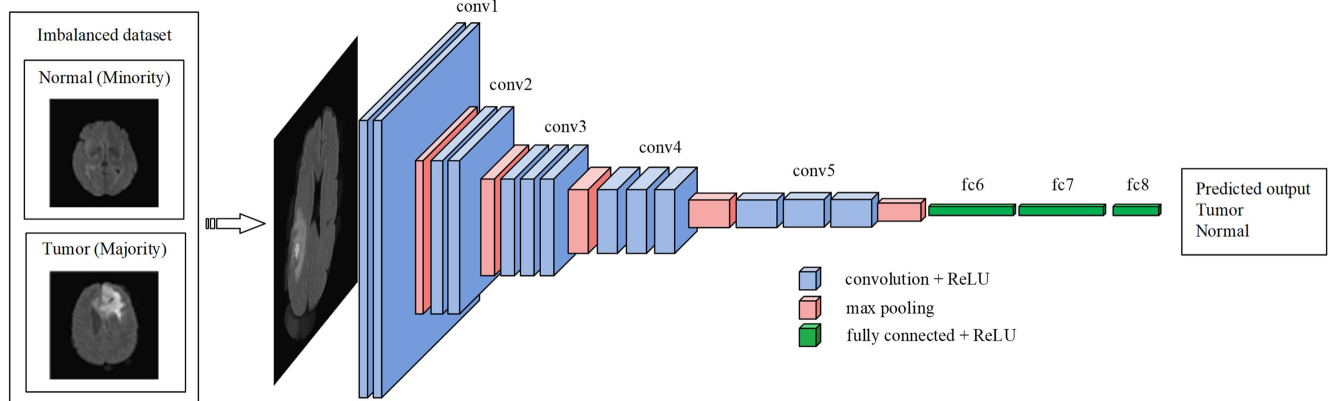


FIGURE 8. Block diagram for training imbalanced dataset.

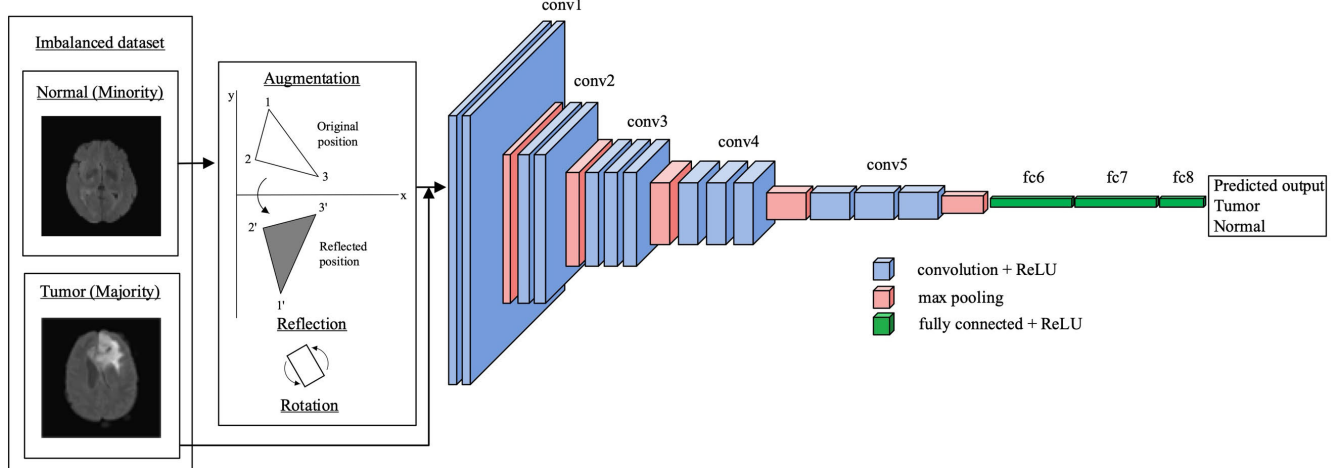


FIGURE 9. Block diagram for training balanced dataset.

the final label of the class with the highest number of voting classes, as shown in Fig. 10.

Majority soft voting: Summing the per-class probability values generated by every classifier for the input image, and obtaining the final label of the class with the greatest probability sum, as shown in Fig. 10.

4) VISUALIZATION USING GRAD-CAM

In this study, Grad-CAM was used to visualize the discriminative regions of the predicted MRI images. A customized program was established according to the block diagram shown in Fig. 11. The trained model from each CNNs algorithm was loaded into the workspace, and a particular image that required visualization and inspection was read into the workspace for further processing. A particular image was classified using the trained model algorithm to predict normal or glioma brain tumors and the probability was indicated. Finally, the predicted results were interpreted using the Grad-CAM algorithm and a heatmap image was generated

for visualization. The pseudocode for the visualization of a particular image is presented in Table 6.

The implementation of this customized program will assist the medical staff in diagnosing glioma brain tumors using individual MRI medical images. The medical MRI image, which was pre-processed as explained in the previous section, was loaded into the workspace. The CNN-trained model predicts an individual image to indicate a tumor or a normal tissue. The predicted images were verified by using the Grad-CAM algorithm.

B. PERFORMANCE EVALUATION

The experimental results were evaluated using the following diagnostic test attributes: sensitivity, specificity, and accuracy, which are widely used to describe diagnostic tests [42]. Several terms were used to describe sensitivity, specificity, and accuracy. These included true positives (TP), true negatives (TN), false negatives (FN), and false positives (FP). In this study, if a tumor was proven to be present in

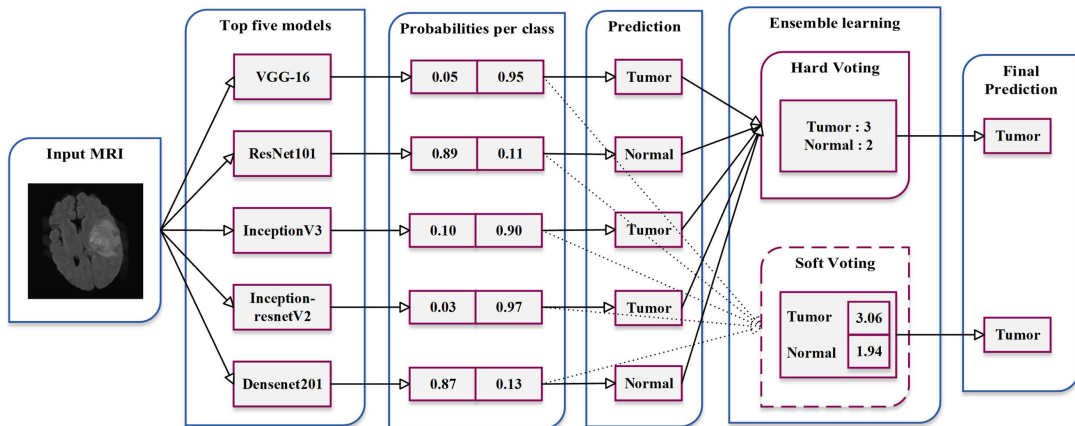


FIGURE 10. Ensemble learning using majority voting.

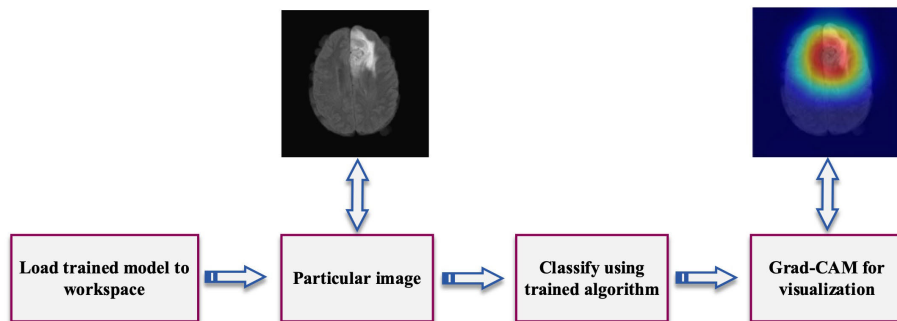


FIGURE 11. Block diagram for visualization using Grad-CAM.

TABLE 6. Pseudo code for classification and visualization of the particular image.

Pseudo-code for image visualization

```

Begin
Require: CNN trained model using a brain tumor training dataset
with transfer learning.
1. Load the CNN trained model to the workspace.
2. Verify the compatibility of the input image size, i.e., the
required input image is 299 x 299 for inceptionV3.
3. Read the input image RGB type, which requires prediction
and visualization into the workspace.
4. The input image was resized to equal the required input
image of the network.
5. The input image is classified to indicate the tumor or
normal brain using the trained model network.
6. Compute the Grad-CAM map to visualize the predicted
image :

$$L_{Grad-CAM}^c = ReLU \left( \sum_k \alpha_k^c A^k \right)$$

7. Displays the discriminative image region of the classified
image.
End

```

a patient, the predicted result indicated the presence of the disease, and the result of the diagnostic test was considered true positive. Similarly, if a tumor was proven to be absent

in a patient, the predicted result indicated that the tumor was absent, and the test result was considered true negative.

True positive and negative results suggest a consistent result between the diagnostic test and the proven condition. In contrast, if a tumor was proven to be present in a patient who had no such disease, the test result was considered a false-positive. Similarly, if a predicted result indicated that a tumor was absent in a patient with a brain tumor, the test result was considered a false-negative. False positives and negatives indicated that the test results were opposite to the actual conditions.

Sensitivity, specificity, and accuracy are described in terms of TP , TN , FN , and FP .

$$Sensitivity = \frac{TP}{(TP + FN)} \quad (11)$$

$$Specificity = \frac{TN}{(TN + FP)} \quad (12)$$

$$Accuracy = \frac{(TP + TN)}{(TP + TN + FN + FP)} \quad (13)$$

The numerical value of sensitivity represents the probability of a diagnostic test identifying patients with the disease. A test with high sensitivity tends to capture all possible positive conditions without missing anyone. Hence, high-sensitivity tests are often used to screen for disease.

TABLE 7. Classification results (Approach 1: imbalanced dataset).

CNNs	Accuracy	Sensitivity	Specificity	AUC
VGG16	92.47%	99.61%	76.52%	0.9961
VGG19	95.70%	99.22%	87.83%	0.9978
ResNet50	94.09%	99.22%	82.61%	0.9957
ResNet101	94.35%	99.22%	83.48%	0.9948
Xception	93.01%	98.44%	80.87%	0.9774
InceptionV3	94.89%	99.61%	84.35%	0.9973
InceptionResNetV2	95.43%	98.05%	89.57%	0.9925
Densenet201	93.55%	98.44%	82.61%	0.9912

The numerical value of the specificity represents the probability of a diagnostic test identifying patients without such diseases. A test with high specificity when conducting a diagnostic test in a patient without a certain disease has a high probability of being identified as negative.

The obtained prediction result is the true positive rate (TPR), which is equivalent to the sensitivity, and the false positive rate (FPR), which is equivalent to $(1 - \text{specificity})$. The all-possible combination of TPR and FPR comprises a Receiver Operating Characteristic (ROC) space. The area under the ROC curve (AUC) was used to measure the accuracy of the diagnostic test. A larger area indicated a more accurate diagnostic test. The AUC of the ROC curve can be measured using the following equation, where $t = (1 - \text{specificity})$ and $\text{ROC}(t)$ is the sensitivity:

$$AUC = \int_0^1 \text{ROC}(t)dt \quad (14)$$

V. RESULTS AND DISCUSSION

In this study, we implemented three different approaches for classifying glioma brain tumors using various CNNs transfer-learning methods and ensemble majority voting, as previously described. In Approach 1, preprocessed MRI images without augmentation were utilized for training and testing using eight CNNs. Finally, the prediction results were used to measure the accuracy and quality of diagnostic tests. The experimental results indicated that VGG19 was the best classifier, with an accuracy of 95.70%, sensitivity of 99.22%, specificity of 87.83%, and AUC of 0.9978. The sensitivity, specificity, accuracy, and AUC of each CNNs classifier are presented in Table 7. The training and testing inference times for each CNNs are presented in Table 8. An example of the ROC curve plotted against the relative true-positive and false-positive rates for the imbalanced dataset is shown in Fig. 12.

In Approach 2, the accuracy and quality of the diagnostic test were significantly improved by using image augmentation to increase the number of images of minority classes. As described in the previous section, an image augmentation methodology and balanced training dataset were implemented to address the imbalanced dataset problem.

TABLE 8. Training and testing inference time for imbalanced dataset.

CNNs	Training elapsed time	Testing inference time
VGG16	7 min. 53 sec.	4.578 seconds
VGG19	8 min. 43 sec.	4.764 seconds
ResNet50	9 min. 33 sec.	5.221 seconds
ResNet101	16 min. 42 sec.	6.312 seconds
Xception	15 min. 10 sec.	6.658 seconds
InceptionV3	14 min. 29 sec.	5.924 seconds
InceptionResNetV2	43 min. 45 sec.	9.445 seconds
Densenet201	42 min. 51 sec.	9.859 seconds

The experimental results showed that all the performance parameters were significantly improved for the almost perfect binary classification of glioma brain tumors. As previously explained, we implemented various CNNs for the training dataset using the algorithm option to obtain the trained model. The training progress is plotted to monitor the accuracy and loss of the validation dataset. Fig. 13 shows the training progress plotted for the best classifier that was InceptionV3. The training progress indicated the validation accuracy. InceptionV3 had a validation accuracy of 99.51%. The trained model was then used to classify glioma brain tumors.

The best CNN classifier was InceptionV3, which achieved an accuracy of 99.73%, a sensitivity of 99.61%, a specificity of 100%, and an AUC of 1. Another CNNs classifier and ensemble majority voting showed the experimental results listed in Table 9. The training and testing inference times for each CNNs are presented in Table 10. The relative between the true positive rate (TPR) and false positive rate (FPR) was used to plot the ROC curve. An example of an ROC curve for a balanced dataset is shown in Fig. 14.

Notably, the InceptionV3 classifier with a balanced dataset obtained the best performance, and Densenet201 obtained very good performance with an accuracy of 99.46%, sensitivity of 99.22%, and specificity of 100%. However, InceptionV3 requires a training time of 25 min. 15 sec. and a testing inference time of 5.878 s, which was less than that of the Densenet201 classifier, which used a training time of 57 min. 25 sec. and a testing inference time of 9.413 s. This is because of the differences in network layers and architectures. In this study, we used a laptop with a CPU Intel Core i7, 3.0 GHz, RAM 32 GB, and an NVIDIA GeForce RTX 3070 graphics processing unit (GPU) for training and testing the brain tumor CNNs.

In Approach 3, to further investigate the efficiency of classification, ensemble learning using majority hard and soft voting, which is a straightforward methodology, was conducted, and the network was not required for training

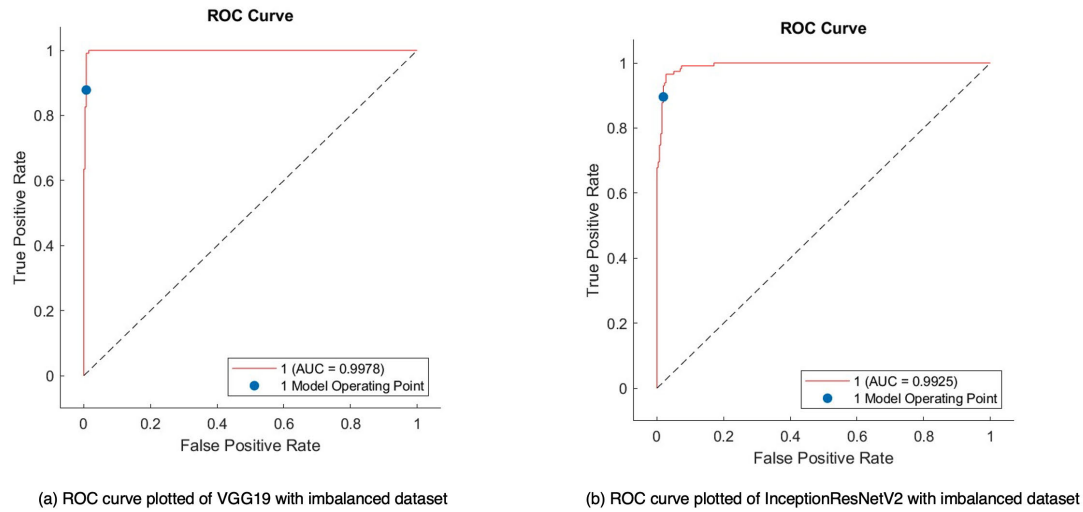


FIGURE 12. ROC curve plotted of classifiers with imbalanced dataset.

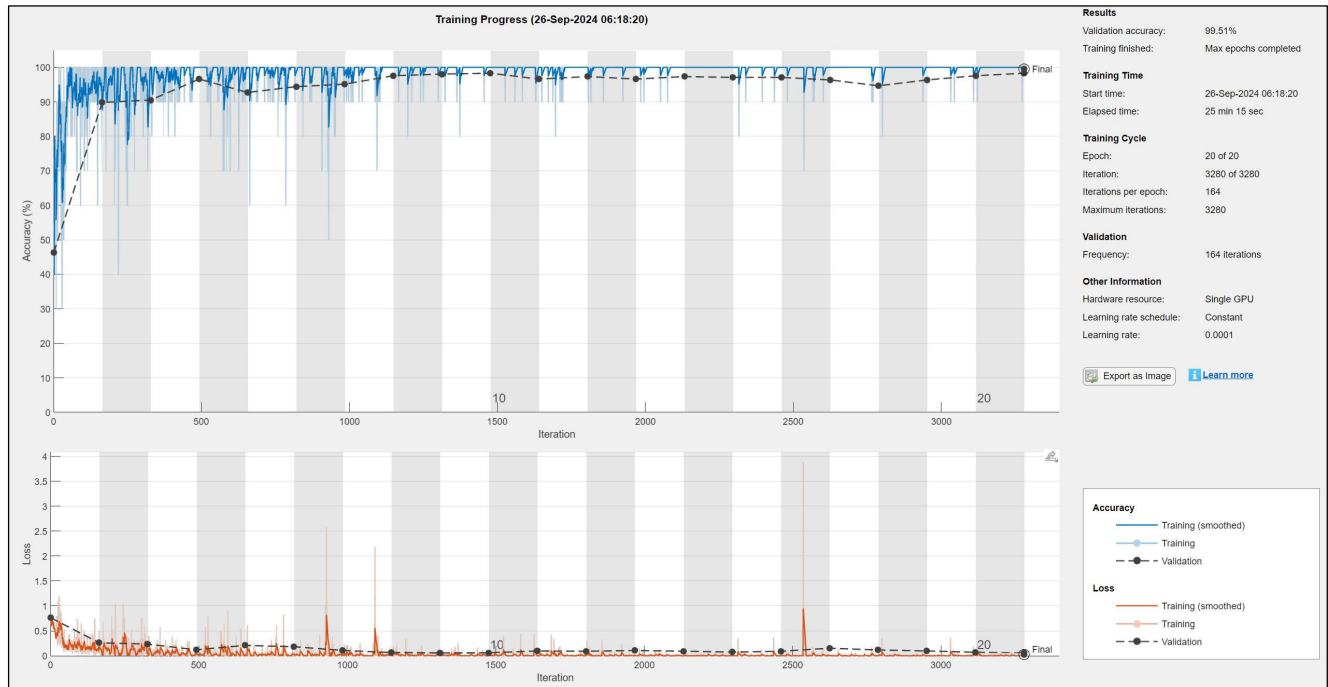


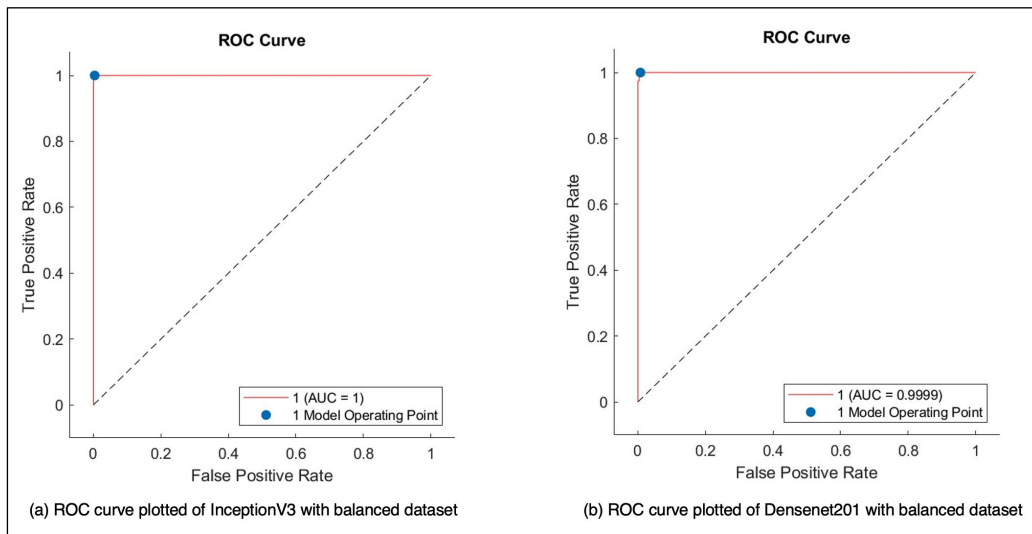
FIGURE 13. Training progress of InceptionV3 with a balanced dataset.

again. The top five classifiers with the best performances were used for majority voting.

Therefore, VGG16, InceptionV3, InceptionResNetV2, ResNet101, and DenseNet201 with a balanced dataset from Approach 2 were utilized. In the hard-voting approach, the predicted label from each classifier was used for summing and voting. In the soft voting approach, the probability per class from each classifier is used for summing and voting, as shown in Fig. 10. Finally, we obtained the evaluated performance from majority voting with an accuracy of

99.46%, a sensitivity of 99.22%, and a specificity of 100%, as shown in Table 9.

Although we present the performance evaluation in Table 9, it is adequate to justify and compare the performances of different classifiers. Furthermore, we propose a quantitative analysis with appropriate statistical testing p-values to evaluate the testing results from each classifier. The p-value represents the probability of observing the sample given that the hypothesis is true. The null hypothesis (H_0) was rejected if the p-value was lower than the significance

**FIGURE 14.** ROC curve plotted of classifiers with balanced dataset.**TABLE 9.** Classification results (Approach 2: balanced dataset).

CNNs	Accuracy	Sensitivity	Specificity	AUC
VGG16	99.19%	99.61%	98.26%	0.9993
VGG19	98.12%	98.83%	96.52%	0.9994
ResNet50	97.85%	98.44%	96.52%	0.9982
ResNet101	99.19%	98.83%	100%	0.9999
Xception	98.12%	98.83%	96.52%	0.9980
InceptionV3	99.73%	99.61%	100%	1.000
InceptionResNetV2	98.66%	98.05%	100%	0.9989
Densenet201	99.46%	99.22%	100%	0.9999
Hard voting	99.46%	99.22%	100%	-
Soft voting	99.46%	99.22%	100%	-

TABLE 10. Training and testing inference time for balanced dataset.

CNNs	Training elapsed time	Testing inference time
VGG16	11 min. 2 sec.	5.955 seconds
VGG19	12 min. 7 sec.	4.884 seconds
ResNet50	12 min. 50 sec.	5.412 seconds
ResNet101	23 min. 21 sec.	6.62 seconds
Xception	27 min. 19 sec.	6.625 seconds
InceptionV3	25 min. 15 sec.	5.878 seconds
InceptionResNetV2	61 min. 3 sec.	9.315 seconds
Densenet201	57 min. 25 sec.	9.413 seconds

level [43]. We used a one-sided test with $H_0 \geq 99$, meaning the probability of prediction result must be greater than or equal to 0.99 for all actual classes, with a significance level

TABLE 11. Statistical testing of classifiers for quantitative analysis.

CNNs	Test statistic	Confidence interval	p-value	Reject H_0
VGG16	0.0068	0.9972	0.5027	0
ResNet101	-0.1454	0.9947	0.4422	0
InceptionV3	-0.0018	0.9943	0.4993	0
InceptionResNetV2	-1.5617	0.9905	0.0596	0
Densenet201	0.2697	0.9966	0.6062	0

of 5% for testing, which led to a critical value of -1.649 . The statistical test results for the top five performance classifiers are presented in Table 11. When rejecting H_0 , if indicated as zero, we cannot reject the null hypothesis. The results indicate that all proposed classifiers have p-values greater than the significance level. Therefore, the null hypothesis is not rejected.

Finally, Grad-CAM was used to visualize the discriminative image region, and interpretability was performed to determine the parts of the image that were the most important for classification. The heatmap shows red color for the region that was most relative to the tumor. The visualization of the indicative region for transparency reflects the reliability and trustworthiness of the classifier.

In this study, we conducted customized programming to implement the Grad-CAM algorithm to visualize particular images for monitoring and to further justify the predicted result, as described in the block diagram in Fig. 11 and the pseudocode in Table 6.

As previously explained, inceptionV3 with a balanced dataset, was the best classifier in our methodology. Hence, the Grad-CAM algorithm using inceptionV3 with a balanced dataset approach was used to visualize the discriminative

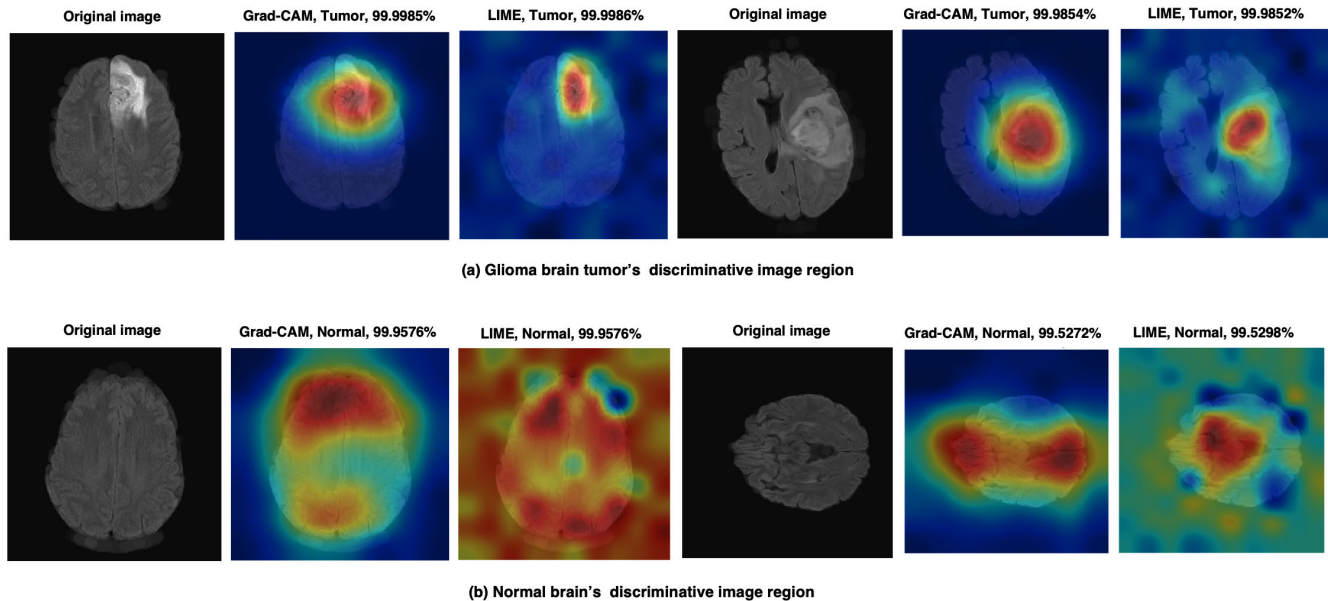


FIGURE 15. Comparison between Grad-CAM and LIME for visualization using InceptionV3.

image regions of the normal brain and tumor; the results are shown in Fig. 15.

We also analyzed the visualization and interpretability of our proposed classifier using the local interpretable model-agnostic explanation (LIME) methodology with InceptionV3, as shown in Fig. 15. This approach ensures that our classifier accurately identifies the discriminative regions of the brain tumors. The visualization process is similar to that of the Grad-CAM algorithm, as explained by the pseudocode in Table 6. However, the map was generated using the LIME algorithm [44].

The experimental results obtained in this study were evaluated and compared with those obtained in previous studies. Our proposed methodology yielded fascinating experimental results. Many previous studies have reported high accuracy in brain tumor classification. However, the trustworthiness and reliability of the classifier are significant and the overfitting problem is a constraint that should be investigated further.

Therefore, the proposed methodology was implemented using two different datasets and the number of images was increased to prevent overfitting. The proposed methodology obtained high performance, and InceptionV3 with a balanced dataset was the best classifier, with an accuracy of 99.73%, sensitivity of 99.61%, specificity of 100%, and AUC of 1.00. Moreover, we implemented the Grad-CAM algorithm to visualize the discriminative image region, which indicated the trustworthiness of the classifier.

VI. CONCLUSION

In this study, we introduce an automated classification method for glioma brain tumors using deep learning CNNs.

MRI images from two different databases were combined and used for the binary classification. Preprocessing with a morphological operation to remove the skeleton and artifacts from the brain region and the CLAHE algorithm to enhance the image contrast were performed. The obtained image dataset was highly imbalanced between glioma tumor and normal brain images, which is the minority class. Therefore, two approaches were implemented to prepare the training dataset: imbalanced and balanced MRI.

An image-augmentation methodology was used to increase the number of minority classes to balance the training dataset. Eight state-of-the-art deep learning CNNs were implemented for the binary classification of glioma brain tumors. The experimental results indicated that the accuracy was significantly improved with an approachable balanced dataset. The top five performance classifier was used for ensemble learning using majority hard and soft voting for further investigation as well. The performance and quality of the experimental results were evaluated, and it was found that better than previous related work, the best classifier for our studied was inceptionV3 with a balanced dataset with an accuracy of 99.73%, sensitivity of 99.61%, specificity of 100%, and area under the ROC curve of 1.00. An appropriate statistical analysis was implemented to evaluate the results from different classifiers, and it was found that the top five performance classifiers selected met the criteria for null hypothesis testing. Additionally, Grad-CAM was implemented to visualize the discriminative image region between the tumor blob and brain region to ensure the trustworthiness of the results predicted by the CNNs classifier. The proposed methodology precisely classifies glioma brain tumors and we envision that our proposed

algorithm will be further improved to assist medical experts in diagnosing brain tumors. In future work, transformer-based models for 3D medical imaging will be investigated to improve the performance of brain tumor classification.

REFERENCES

- [1] S. Bauer, R. Wiest, L.-P. Nolte, and M. Reyes, "A survey of MRI-based medical image analysis for brain tumor studies," *Phys. Med. Biol.*, vol. 58, no. 13, p. R97, Jul. 2013.
- [2] D. N. Louis, A. Perry, G. Reifenberger, A. von Deimling, D. Figarella-Branger, W. K. Cavenee, H. Ohgaki, O. D. Wiestler, P. Kleihues, and D. W. Ellison, "The 2016 world health organization classification of tumors of the central nervous system: A summary," *Acta Neuropathologica*, vol. 131, no. 6, pp. 803–820, Jun. 2016.
- [3] H. T. Zaw, N. Maneerat, and K. Y. Win, "Brain tumor detection based on Naïve Bayes classification," in *Proc. 5th Int. Conf. Eng., Appl. Sci. Technol. (ICEAST)*, Luang Prabang, Laos, Jul. 2019, pp. 1–4.
- [4] P. Pilaoon, N. Maneerat, K. Yajima, R. Varakulsiripunth, and K. Hamamoto, "Brain tumor classification using supervised support vector machine," in *Proc. 9th Int. Conf. Eng., Appl. Sci., Technol. (ICEAST)*, Vientiane, Laos, Jun. 2023, pp. 79–83.
- [5] Y. K. Dubey, M. M. Mushrif, and K. Pisar, "Brain tumor type detection using texture features in MR images," in *Proc. IEEE Region Humanitarian Technol. Conf.*, Dec. 2018, pp. 1–4.
- [6] P. Pilaoon, N. Maneerat, A. Nakthewan, R. Varakulsiripunth, and K. Hamamoto, "Brain tumor classification using pretrained deep convolutional neural network," in *Proc. 9th Int. Conf. Eng., Appl. Sci., Technol. (ICEAST)*, Vientiane, Laos, Jun. 2023, pp. 84–88.
- [7] T. Hossain, F. S. Shishir, M. Ashraf, M. A. A. Nasim, and F. M. Shah, "Brain tumor detection using convolutional neural network," in *Proc. 1st Int. Conf. Adv. Sci., Eng. Robot. Technol. (ICASERT)*, May 2019, pp. 1–6.
- [8] N. M. Dipu, S. A. Shohan, and K. M. A. Salam, "Deep learning based brain tumor detection and classification," in *Proc. Int. Conf. Intell. Technol. (CONIT)*, Karnataka, India, Jun. 2021, pp. 1–6.
- [9] S. Arora and M. Sharma, "Deep learning for brain tumor classification from MRI images," in *Proc. 6th Int. Conf. Image Inf. Process. (ICIIP)*, vol. 6, Nov. 2021, pp. 409–412.
- [10] S. Gaikwad, S. Patel, and A. Shetty, "Brain tumor detection: An application based on machine learning," in *Proc. 2nd Int. Conf. Emerg. Technol. (INCET)*, Belgaum, India, May 2021, pp. 1–4.
- [11] S. K. Baranwal, K. Jaiswal, K. Vaibhav, A. Kumar, and R. Srikantawamy, "Performance analysis of brain tumour image classification using CNN and SVM," in *Proc. 2nd Int. Conf. Inventive Res. Comput. Appl. (ICIRCA)*, Jul. 2020, pp. 537–542.
- [12] I. Aboussaleh, J. Riffi, A. M. Mahraz, and H. Tairi, "Brain tumor segmentation based on deep learning's feature representation," *J. Imag.*, vol. 7, no. 12, p. 269, Dec. 2021.
- [13] A. Younis, L. Qiang, C. O. Nyatega, M. J. Adamu, and H. B. Kauwua, "Brain tumor analysis using deep learning and VGG-16 ensembling learning approaches," *Appl. Sci.*, vol. 12, no. 14, p. 7282, Jul. 2022.
- [14] H. Hu, X. Li, W. Yao, and Z. Yao, "Brain tumor diagnose applying CNN through MRI," in *Proc. 2nd Int. Conf. Artif. Intell. Comput. Eng. (ICAICE)*, Nov. 2021, pp. 430–434.
- [15] S. Pereira, A. Pinto, V. Alves, and C. A. Silva, "Brain tumor segmentation using convolutional neural networks in MRI images," *IEEE Trans. Med. Imag.*, vol. 35, no. 5, pp. 1240–1251, May 2016.
- [16] H. Kibriya, M. Masood, M. Nawaz, R. Rafique, and S. Rehman, "Multiclass brain tumor classification using convolutional neural network and support vector machine," in *Proc. Mohammad Ali Jinnah Univ. Int. Conf. Comput. (MAJICC)*, Jul. 2021, pp. 1–4.
- [17] A. W. Reza, M. S. Hossain, M. A. Wardiful, M. Farzana, S. Ahmad, F. Alam, R. N. Nandi, and N. Siddique, "A CNN-based strategy to classify MRI-based brain tumors using deep convolutional network," *Appl. Sci.*, vol. 13, no. 1, p. 312, Dec. 2022.
- [18] S. Asif, W. Yi, Q. U. Ain, J. Hou, T. Yi, and J. Si, "Improving effectiveness of different deep transfer learning-based models for detecting brain tumors from MR images," *IEEE Access*, vol. 10, pp. 34716–34730, 2022.
- [19] S. Mohsen, A. M. Ali, E.-S.-M. El-Rabaie, A. ElKaseer, S. G. Scholz, and A. M. A. Hassan, "Brain tumor classification using hybrid single image super-resolution technique with ResNext101_32x_8d and VGG19 pre-trained models," *IEEE Access*, vol. 11, pp. 55582–55595, 2023.
- [20] REMBRANDT. (2017). *The Cancer Imaging Archive*. [Online]. Available: <https://wiki.cancerimagingarchive.net/display/Public/REMBRANDT>
- [21] U. Baid et al., "The RSNA-ASNR-MICCAI BraTS 2021 benchmark on brain tumor segmentation and radiogenomic classification," 2021, *arXiv:2107.02314*.
- [22] B. H. Menze et al., "The multimodal brain tumor image segmentation benchmark (BRATS)," *IEEE Trans. Med. Imag.*, vol. 34, no. 10, pp. 1993–2024, Oct. 2015, doi: [10.1109/TMI.2014.2377694](https://doi.org/10.1109/TMI.2014.2377694).
- [23] S. Bakas, H. Akbari, A. Sotiras, M. Bilello, M. Rozycski, J. S. Kirby, J. B. Freymann, K. Farahani, and C. Davatzikos, "Advancing the cancer genome atlas glioma MRI collections with expert segmentation labels and radiomic features," *Sci. Data*, vol. 4, no. 1, pp. 1–13, Sep. 2017, doi: [10.1038/sdata.2017.117](https://doi.org/10.1038/sdata.2017.117).
- [24] R. Gonzalez and R. Woods, *Digital Image Processing*, 4th ed., London, U.K.: Pearson, 2018.
- [25] R. Gonzalez, R. Woods, and S. Eddins, *Digital Image Processing Using MATLAB*, 2nd ed., London, U.K.: Pearson, 2017.
- [26] S. M. Pizer, E. P. Amburn, J. D. Austin, R. Cromartie, A. Geselowitz, T. Greer, B. T. H. Romeny, J. B. Zimmerman, and K. Zuiderveld, "Adaptive histogram equalization and its variations," *Comput. Vis., Graph., Image Process.*, vol. 39, no. 3, pp. 355–368, Sep. 1987.
- [27] K. Zuiderveld, "Contrast limited adaptive histogram equalization," in *Graphics Gems IV*, vol. 1994. Cambridge, U.K.: Academic, 1994, pp. 474–485.
- [28] I. Valova, C. G. Harris, T. Mai, and N. Gueorguieva, "Optimization of convolutional neural networks for imbalanced set classification," in *Proc. 24th Int. Conf. KES*, Jan. 2020, pp. 660–669.
- [29] K. Y. Win, N. Maneerat, S. Sreng, and K. Hamamoto, "Ensemble deep learning for the detection of COVID-19 in unbalanced chest X-ray dataset," *Appl. Sci.*, vol. 11, no. 22, p. 10528, Nov. 2021.
- [30] J. Nalepa, M. Marcinkiewicz, and M. Kawulok, "Data augmentation for brain-tumor segmentation: A review," *Frontiers Comput. Neurosci.*, vol. 13, Dec. 2019, Art. no. 83.
- [31] I. Goodfellow, Y. Bengio, and A. Courville, *Deep Learning*. Cambridge, MA, USA: MIT Press, 2017, pp. 294–299.
- [32] K. Simonyan and A. Zisserman, "Very deep convolutional networks for large-scale image recognition," in *Proc. 3rd Int. Conf. Learn. Represent.*, San Diego, CA, USA, May 2015, pp. 1–8.
- [33] K. He, X. Zhang, S. Ren, and J. Sun, "Deep residual learning for image recognition," in *Proc. IEEE Conf. Comput. Vis. Pattern Recognit. (CVPR)*, Jun. 2016, pp. 770–778.
- [34] F. Chollet, "Xception: Deep learning with depthwise separable convolutions," in *Proc. IEEE Conf. Comput. Vis. Pattern Recognit. (CVPR)*, Jul. 2017, pp. 1800–1807.
- [35] C. Szegedy, V. Vanhoucke, S. Ioffe, J. Shlens, and Z. Wojna, "Rethinking the inception architecture for computer vision," in *Proc. IEEE Conf. Comput. Vis. Pattern Recognit. (CVPR)*, Jun. 2016, pp. 2818–2826.
- [36] C. Szegedy, S. Ioffe, V. Vanhoucke, and A. A. Alemi, "Inception-v4, inception-ResNet and the impact of residual connections on learning," in *Proc. 31st AAAI Conf. Artif. Intell.*, San Francisco, CA, USA, Feb. 2017, pp. 4278–4284.
- [37] G. Huang, Z. Liu, L. Van Der Maaten, and K. Q. Weinberger, "Densely connected convolutional networks," in *Proc. IEEE Conf. Comput. Vis. Pattern Recognit. (CVPR)*, Jul. 2017, pp. 2261–2269.
- [38] B. Zhou, A. Khosla, A. Lapedriza, A. Oliva, and A. Torralba, "Learning deep features for discriminative localization," in *Proc. IEEE Conf. Comput. Vis. Pattern Recognit. (CVPR)*, Las Vegas, NV, USA, Jun. 2016, pp. 2921–2929.
- [39] R. R. Selvaraju, M. Cogswell, A. Das, R. Vedantam, D. Parikh, and D. Batra, "Grad-CAM: Visual explanations from deep networks via gradient-based localization," in *Proc. IEEE Int. Conf. Comput. Vis. (ICCV)*, Oct. 2017, pp. 618–626.
- [40] M. Ben Jabra, A. Koubaa, B. Benjdira, A. Ammar, and H. Hamam, "COVID-19 diagnosis in chest X-rays using deep learning and majority voting," *Appl. Sci.*, vol. 11, no. 6, p. 2884, Mar. 2021.

- [41] B. Machura, D. Kucharski, O. Bozek, B. Eksner, B. Kokoszka, T. Pekala, M. Radom, M. Strzelczak, L. Zarudzki, B. Gutiérrez-Becker, A. Krason, J. Tessier, and J. Nalepa, "Deep learning ensembles for detecting brain metastases in longitudinal multi-modal MRI studies," *Computerized Med. Imag. Graph.*, vol. 116, Sep. 2024, Art. no. 102401.
- [42] W. Zhu, N. Zeng, and N. Wang, "Sensitivity, specificity, accuracy, associated confidence interval and ROC analysis with practical SAS implementations," in *Proc. NESUG Health Care Life Sci.*, Baltimore, MD, USA, Nov. 2010, pp. 1–9.
- [43] D. C. Montgomery and G. C. Runger, *Applied Statistics and Probability for Engineers*, 7th ed., Hoboken, NJ, USA: Wiley, 2018, pp. 194–243.
- [44] M. T. Ribeiro, S. Singh, and C. Guestrin, "Why should I trust you?" explaining the prediction of any classifier," in *Proc. 22nd ACM SIGKDD Int. Conf. Knowl. Discovery Data Mining*, 2016, pp. 1135–1144.



PONGSAK PILAOON received the B.Eng. degree in instrumentation engineering and the M.Eng. degree in automation engineering from the King Mongkut's Institute of Technology Ladkrabang (KMITL), Thailand, in 2003 and 2017, respectively, where he is currently pursuing the Ph.D. degree with the School of Engineering. He has authored two research articles. His research interests include medical image classification, deep learning, and machine learning.



KAZUHIKO HAMAMOTO (Member, IEEE) received the B.Eng., M.Eng., and D.Eng. degrees from Tokyo University of Agriculture and Technology, in 1989, 1991, and 1994, respectively. He is currently a Professor with the Department of Information Media Technology, School of Information Science and Technology, Tokai University, Japan. He published around 60 journal/transaction articles and more than 90 international conference papers. His research interests include medical information, human interface design, and virtual reality. He is a member of many national societies in Japan.



NOPPADOL MANEERAT received the B.Sc. degree in physics from Srinakarinwirot University (SWU), Phitsanulok, Thailand, in 1990, and the M.Eng. and D.Eng. degrees in electrical engineering from the King Mongkut's Institute of Technology Ladkrabang (KMITL), Thailand, in 1997 and 2006, respectively. Currently, he is with the Department of Instrumentation and Control Engineering, School of Engineering, KMITL. His research interests include digital image processing, artificial intelligence, and electronic devices.

• • •